

Computational and statistical study on the molecular interaction between antigen and antibody

Tomonori Osajima, Masaaki Suzuki, Saburo Neya, Tyuji Hoshino*

Graduate School of Pharmaceutical Sciences, Chiba University, Inohana 1-8-1, Chuo-ku, Chiba 260-8675, Japan



ARTICLE INFO

Article history:

Accepted 9 July 2014

Available online 23 July 2014

Keywords:

Antibody

Antigen

Complex structure

Binding energy

Molecular dynamics simulation

ABSTRACT

Monoclonal antibodies are one of the most successful bio-molecules utilized in the clinical scene of today. It is important to clarify general characteristics of the interaction between antigen and antibody and to draw a guide for enhancing their binding affinity in rational design of antibody drugs. In this study, we carried out molecular dynamics simulations for 20 kinds of antigen–antibody complexes. From the statistical analysis of the calculation results, the following findings were deduced. At complementarity determining regions (CDRs) of the antibodies, the rates for the presence of serine (Ser) and tyrosine (Tyr) are high. The amino residues involved in direct hydrogen bonds between antigens and antibodies were examined by counting the numbers of the hydrogen bonds from the respective residues. The contribution of Tyr to the direct hydrogen bonding was the highest and that of Ser was the fourth. Furthermore, the short-distance hydrogen bonds, which is assumed to be so-called “low-barrier hydrogen bond”, were observed at CDRs in three complexes. Interestingly, Ser is involved in the short-distance hydrogen bonding in two cases out of the three. This result suggests that these two unchanged polar amino acid residues play an important role for recognition of antigen. In almost all of the complexes (18/20), the contribution of the electrostatic energy (ΔE_{ele}) to the binding free energy was calculated to be larger than that of the van der Waals energy (ΔE_{vdw}). This dominance of the electrostatic energy is in contrast to the case that low molecular-weight compounds are bound to their targets. The findings of this study will be helpful to design an antibody with a high specificity and a high affinity to the antigen.

© 2014 Elsevier Inc. All rights reserved.

1. Introduction

Antibodies occupy an important position in biochemical research, diagnosis, and therapy, in recent years [1,2]. Regarding therapeutics, the contribution of antibody is increasing and nowadays antibody drugs account for one third of all newly approved medicines for cancers, arthritis, asthma, psoriasis, virus infection, transplant rejection, and so on [3–5]. Antibodies are a family of glycoproteins which are specifically bound to the respective antigens. The most remarkable feature of the antigen–antibody interaction is the high specificity and high affinity [6–9]. A binding strength between an antigenic determinant in an antigen (epitope) and an antigen-binding site in an antibody (paratope) is regarded as affinity. The functional strength in combining of antibody with a target protein is termed as avidity. Avidity is a measure of the overall strength of binding of an antigen with many antigenic determinants and multivalent antibodies.

One natural antibody, typically immunoglobulin, has at least two antigen-binding sites. The antigen binding site is usually formed by six polypeptide segments which consist of three variable loops of light chain (L1, L2, and L3) and three variable loops of heavy chain (H1, H2, and H3) [6,7,10]. These six loop segments are highly variable and are named as complementarity-determining regions (CDRs). The local conformational changes called as the induced fit are often observed both for antibody and antigen in their complex, suggesting that the induced fit is important for high specificity and affinity in the antibody–antigen interaction [6].

Lots of three-dimensional structures of the antigen–antibody complexes have already been determined by X-ray crystallographic analysis for a variety of antigen–antibody combinations. In this study, twenty kinds of crystal structures of antigen–antibody complexes were picked up for the computational analysis. In the choice of the twenty complexes, we avoided such crystal structures that antigen part was a linear short peptide or the resolution of X-ray diffraction was not fine. The proteins selected as antigens are influenza virus neuraminidase [11–13], human immunodeficiency virus type 1 (HIV-1) capsid protein [14,15], Taq DNA polymerase [16], hen egg-white lysozyme [17–28], anti-idiotopic

* Corresponding author. Tel.: +81 43 226 2936; fax: +81 43 226 2936.

E-mail address: hoshino@chiba-u.jp (T. Hoshino).

Table 1

Profiles of antigen and antibody for 20 complexes used in the present MD simulations.

PDB code	Antigen	Antibody	Reference
1A14	Influenza virus neuraminidase	NC10	11, 12, 13
1AFV	HIV-1 capsid protein	Fab 25.3	14, 15
1BGX	Taq DNA polymerase (TaqP)	TP7	16
1DQJ	Hen egg-white lysozyme (HEL)	HyHEL-63	17, 18
1DVF	Anti-idiotopic antibody (E5.2)	D1.3	29, 30
1FJ1	Outer surface protein A (OspA)	LA-2	31, 32
1H0D	Human angiogenin (ANG)	Fab 26-2F	33
1IGC	Streptococcal Protein G	Mouse IgG1κ (MOPC21) Fab	34, 35
1IQD	Factor VIII	BO2C11	36, 37
1JPS	Tissue factor	D3H44	38, 39
1KB5	Mouse T-cell receptor (TCR)	Désiré-1 Fab	40, 41
1NDG	HEL	HyHEL-8	19, 20, 21
1NDM	HEL	HyHEL-26	22, 23
1NL0	Factor IX	10C12	42, 43
1UA6	HEL	HyHEL-10	20, 24, 25, 26
2JEL	Histidine-containing phosphocarrier protein (HPr)	Jel42	44, 45
2VIR	Influenza virus hemagglutinin (HA)	Fab	46, 47, 48
2VIS	HA	Fab	46, 47, 48
2VIT	HA	Fab	46, 47, 48
3HFL	HEL	HyHEL-5	27, 28

antibody [29,30], outer surface protein A [31,32], human angiogenin [33], streptococcal protein G [34,35], factor VIII [36,37], tissue factor [38,39], mouse T-cell receptor [40,41], factor IX [42,43], histidine-containing phosphocarrier protein [44,45], and influenza virus hemagglutinin [46–48] as listed in Table 1. These broad examples will provide us the information of epitope, paratope, specificity, affinity, thermodynamic property for the binding interaction between antigens and antibodies.

X-ray crystal structures, however, do not fully satisfy our understanding on the energetic aspect of the binding interaction, for example, van der Waals potential energy, electrostatic energy, and/or contribution of water molecules. Computational study enables us to examine the inter-molecular interaction between proteins, chemical compounds, lipids, ions and so on [49]. Molecular dynamics (MD) simulation is one of the major computational approaches for analyzing the interaction between epitope and paratope and the simulation can predict even a suitable epitope inducing immunological response [49,50]. Now it is important to clarify the general features of the interaction between antigen and antibody in the structural and energetic viewpoints, which will be very helpful to make a strategy to develop a new potent antibody with a high specificity and a high affinity.

The objective of this study is to clarify the dominant factors for the interaction between antigen and antibody. In this study, we performed MD simulations for twenty kinds of antigen–antibody complexes and calculated (i) the averaged three-dimensional structure and root mean squared deviation (RMSD), (ii) the appearance rate of each amino acid residue at CDR to find what amino acid residues are strongly involved in the antigen–antibody binding, (iii) the binding free energy and its energetic components in the antigen–antibody interaction, (iv) the number, distance, and angle of the direct and water molecule-mediated hydrogen bonds at CDR to characterize the hydrogen bonding, (v) the averaged B-factor values of the main chain atoms to examine the flexibility of antibody due to the binding to antigen.

2. Methods

2.1. Construction of computational model

Three-dimensional structures of the antigen–antibody complexes used in this study were extracted from the X-ray crystallographic data in the protein data bank (PDB). The respective

PDB codes are 1A14, 1AFV, 1BGX, 1DQJ, 1DVF, 1FJ1, 1H0D, 1IGC, 1IQD, 1JPS, 1KB5, 1NDG, 1NDM, 1NL0, 1UA6, 2JEL, 2VIR, 2VIS, 2VIT and 3HFL (Table 1). The initial structure of each calculation model was constructed from the atom coordinates of the crystal structure with a modification by adding the missing residues and generating hydrogen atoms. Each complex model was placed in a rectangular periodic-boundary box and solvated with 15,000–60,000 TIP3P water molecules using leap module of AMBER11 program package [51].

2.2. Calculation condition for MD simulation

MD simulation was performed with sander module of AMBER11 program [51]. AMBER ff03 force field was applied. MD simulation was executed in three steps of minimization, heating, and equilibration. Atom geometry was energetically minimized in the first step. The minimization was performed with the steepest descent method for the earlier 3000 cycles and with the conjugated gradient method for the later 10,000 cycles, with only water molecules permitted to move freely. Subsequently, the minimization was performed again in a similar manner without any positional constraint on the atoms [52]. In the heating, the temperature of the calculation system was gradually increased to 300 K in the NVT ensemble condition. Then, the equilibration calculation was performed in the NPT ensemble condition with a temperature of 300 K and a pressure of 1 atm. A periodic boundary condition was applied to all the xyz-directions, and the pressure and the temperature were kept constant. The cutoff distance for van der Waals and Coulomb forces in a real space was set to 12.0 Å. The particle mesh Ewald method was applied to estimate the influence of long-distance electrostatic force. For all of the twenty complexes, 8 ns MD simulation was carried out and the trajectory for the last 1 ns was collected for analysis. Snapshot structures were extracted from the trajectory every 10 ps in order to analyze the average structure, the interaction energy, hydrogen bonding, atom fluctuations.

2.3. Analysis of simulation data

The average structure of each complex was calculated using a trajectory acquired every 10 ps for the last 1 ns of the simulation. All the twenty structures were visualized with PyMOL [53]. The calculations should be sufficiently equilibrated for the sake of reliable analysis. The root mean square deviation (RMSD) is one

of the standard indices to confirm the equilibration. RMSD value during MD simulation was monitored, with respect to the main chain C_α, N, and C atoms.

The appearance probabilities of the respective amino acid residues at CDR of the antibody were calculated for each complex in percentage ratio of number of each amino acid residue to all the amino acid residues at CDR. In addition, the appearances were averaged over all the twenty antibodies to examine whether there exists a preference for the presence of amino acid residues at CDR. Moreover, these appearance probabilities of the residues at CDR of the antibodies were compared with the average presence of amino acid residues among the popular proteins [54] in Swiss-Prot Protein database [55] that was composed of amino acid sequences extracted from more than twenty thousand proteins.

The formation of hydrogen bond was defined in terms of distance and angle. The combination of donor D, hydrogen H, and acceptor A atoms with a D—H···A configuration was regarded as a hydrogen bond when the distance between donor D and acceptor A was shorter than 3.5 Å and the angle H—D—A was smaller than 60.0°. The hydrogen bonds were examined using the trajectory of the last 1 ns simulation and the distances were averaged over the trajectories.

The binding free energy (ΔG_{bind}) was estimated by averaging the binding energies for the snapshot structures acquired every 10 ps of the last 1 ns simulation, using the molecular mechanics-generalized Born surface area (MM-GB/SA) method [56,57]. ΔG_{bind} is obtained as the sum of the three terms:

$$\Delta G_{\text{bind}} = \Delta E_{\text{mm}} + \Delta G_{\text{sol}} - T\Delta S,$$

where ΔE_{mm} , ΔG_{sol} , and $-T\Delta S$ are the change in molecular mechanical energy due to the complex formation, the change in solvation free energy, and the change in conformational entropy, respectively. ΔE_{mm} consists of the three components:

$$\Delta E_{\text{mm}} = \Delta E_{\text{int}} + \Delta E_{\text{ele}} + \Delta E_{\text{vdw}},$$

where ΔE_{int} , ΔE_{ele} , and ΔE_{vdw} are the internal elastic energy, the electrostatic energy, and the van der Waals energy, respectively. Hence, ΔG_{bind} is evaluated from the following equation:

$$\Delta G_{\text{bind}} = \Delta E_{\text{int}} + \Delta E_{\text{ele}} + \Delta E_{\text{vdw}} + \Delta G_{\text{sol}} - T\Delta S.$$

$-T\Delta S$ were set as 0.0 in our present study because the main purpose of this study is to clarify the energetic contribution from the electrostatic and/or the van der Waals forces in the antigen–antibody interaction. The influence of the entropic term on the molecular binding has already been discussed in the other work [49]. Hence, we decided to disregard the entropic term because our present study is not to compare the binding free energies among the twenty complexes. ΔG_{sol} is further divided into the two terms:

$$\Delta G_{\text{sol}} = \Delta G_{\text{GB}} + \Delta G_{\text{SA}},$$

where ΔG_{GB} is the electrostatic solvation energy and ΔG_{SA} is a non-polar solvation energy. ΔG_{GB} was computed by the generalized Born method with the mmpbsa module [58] of the AMBER 11. In this study, the dielectric constant was set to 1.0 for the interior solute and 80.0 for the exterior solvent. ΔG_{SA} was obtained by the equation:

$$G_{\text{SA}} = \gamma \times \text{SASA} + \beta,$$

where γ is the surface tension constant and was set to 0.0072 kcal/(mol Å²), and β is the offset value, which was 0.0 here. The solvent-accessible surface area (SASA) was determined with the linear combination of pairwise overlaps (LCPO) model [59].

Fluctuations of the main chain atoms, C_α, C, and N, were calculated by the deviations from their average positions, using ptraj

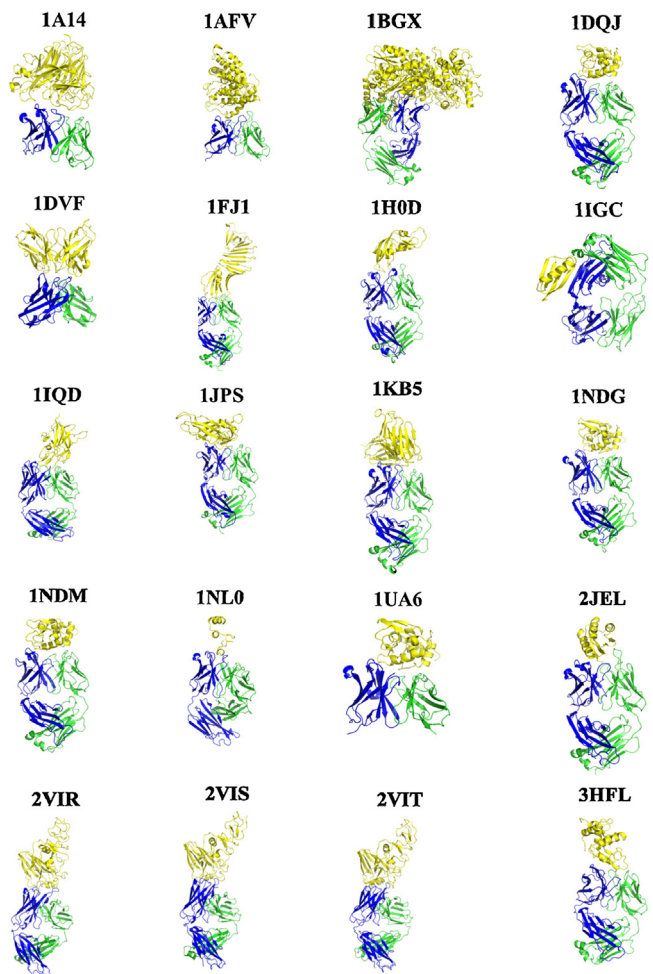


Fig. 1. Average structures obtained from the MD simulations for 20 kinds of the antigen–antibody complexes. The antigen was colored yellow. The heavy and light chains of the antibody is represented by blue and green ribbons, respectively.

module of AMBER11. The calculated deviations were averaged for each amino acid residue to evaluate the B-factor value [60,61].

3. Results

3.1. Complex structures

The RMSDs of main chain atoms in all the complexes were calculated to confirm the equilibration of the simulations and to examine the dynamic stability of the complexes (Fig. S1 in supporting information). The model system was judged to be equilibrated because the fluctuation of the RMSD was smaller than 2 Å during the last 1 ns simulation. Since no abrupt change in RMSD was observed, the trajectories of the complexes are assumed to be stable in spite of small fluctuations in 1JPS, 1KB5, 2VIR, 2VIT. The average structures of the twenty complexes for the last 1 ns are illustrated without water molecules in Fig. 1. In the complexes for 1A14, 1AFV, 1DVF and 1UA6, the antibodies are in the form of single-chain variable fragment (scFv). The antibodies for the other complexes are in the form of fragment antigen-binding (Fab). The loop regions of the antibodies are responsible for the binding to the antigens, while not the loop region but the α-helix domain is bound to the antigen in 1IGC.

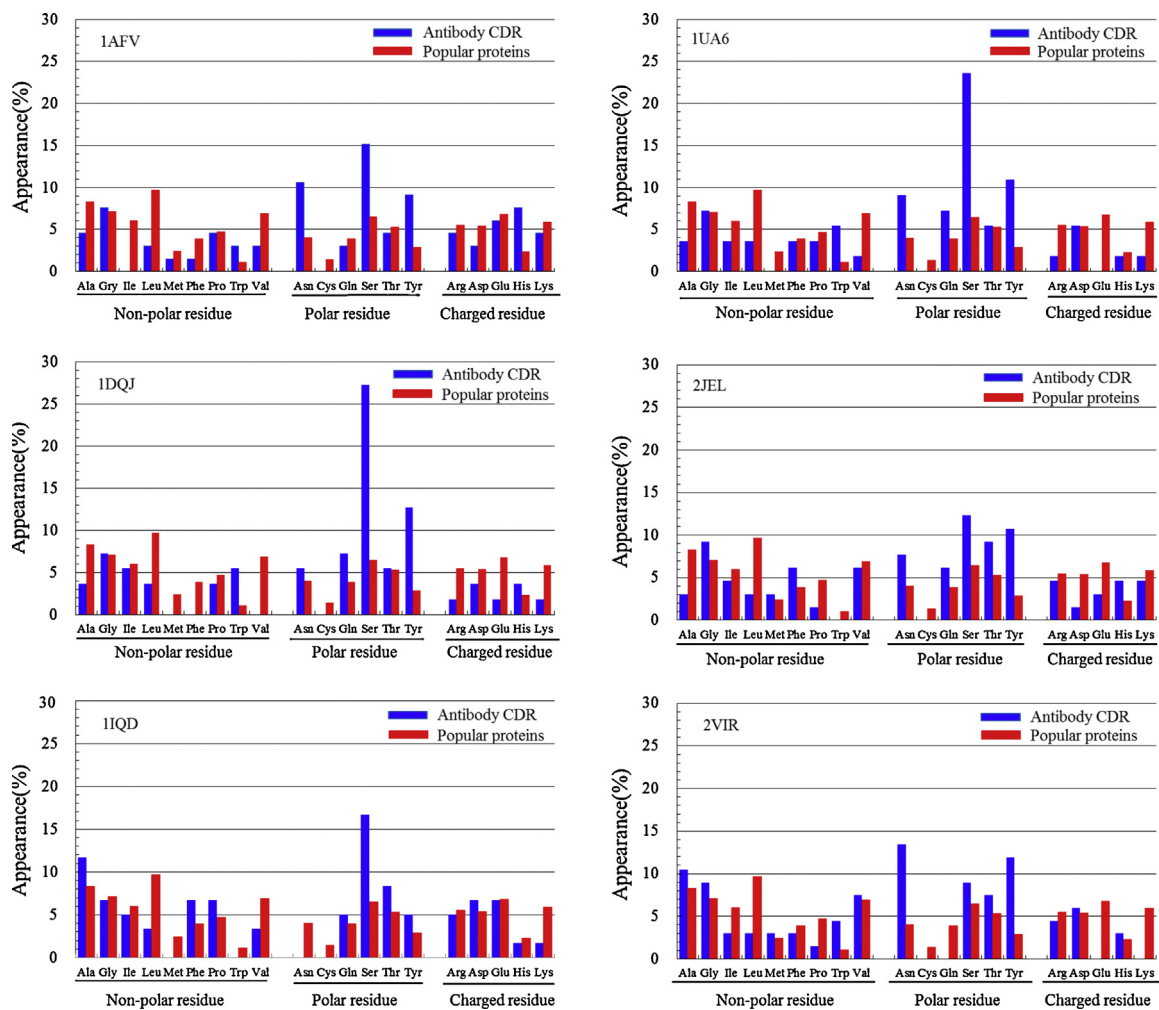


Fig. 2. Appearance rates of amino acid residues at the CDR of antibodies for 6 kinds of complexes selected as typical examples.

3.2. Amino acid residues at CDR of antibody

The ratio of the presence of amino acid residues at CDR was calculated for each antibody. The presence of amino residues in the popular proteins was also shown to compare with that of the twenty antibodies. The calculated percentage ratios are shown in Fig. S2 of supporting information for all the complexes. Hereafter, we selected 6 complexes; PDB code: 1AFV, 1DQJ, 1IQD, 1UA6, 2JEL and 2VIR, as typical examples in the main text of this paper. In this selection, 1AFV and 1UA6 are in the scFv form whereas 1DQJ, 1IQD, 2JEL and 2VIR are in the Fab form. In the two scFv complexes, the secondary structure of the local region of the antigen in contact with CDR is α -helix for 1AFV while that is β -turn for 1UA6. In the four complexes of the Fab form, the local regions of the antigens in contact with CDR are α -helix for 1DQJ and 2VIR, β -sheet for 1IQD, and β -turn for 2JEL. In all the example complexes, the contact regions of the antigens are located at the middle of CDR of the antibodies.

The presence ratios for these 6 complexes are shown in Fig. 2. The presences of Asn, Gln, Ser, Tyr and Thr are high at CDR of antibodies, compared with those in the popular proteins. All these 5 amino acid residues have a polar side chain without electric charge. In particular, the appearance rates for both Ser and Tyr were outstanding. The antibodies in 1DQJ and 1UA6 are named as HyHEL-63 and HyHEL-10, respectively, and the antigen of both these antibodies is hen egg-white lysozyme, HEL. The appearance of the residue was 27.3% for Ser and 12.7% for Tyr in 1DQJ and was 23.6% for Ser and 10.9% for Tyr in 1UA6. In the Fab antibodies of 1AFV and 2VIR,

the antigens of which were derived from viruses, also show high appearances for Ser, Tyr, and Asn. In 2JEL, the appearances of Ser, Thr, and Tyr were observed to be remarkably high. In 1IQD, the antigen is a blood coagulation factor III and the antibody is named as BO2C11. In 1IOD, only Ser showed a high appearance.

The averaged presences of the respective amino acid residues at CDR for the twenty complexes are illustrated in Fig. 3. The appearances of Tyr and Ser are remarkably high, suggesting that there is a specific preference for the presence of amino acid residues at CDR

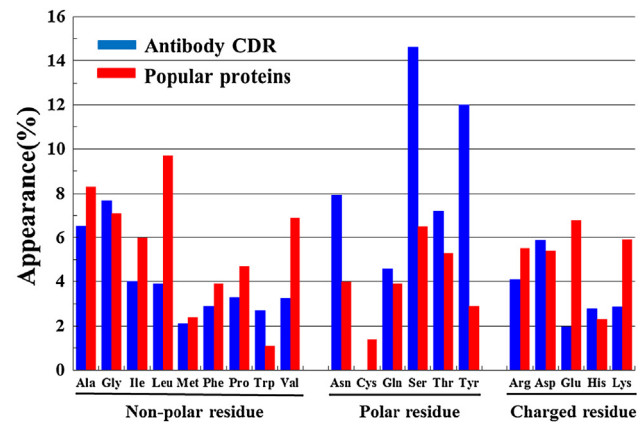


Fig. 3. Presences of amino acid residues at the CDR, averaged over the 20 complexes.

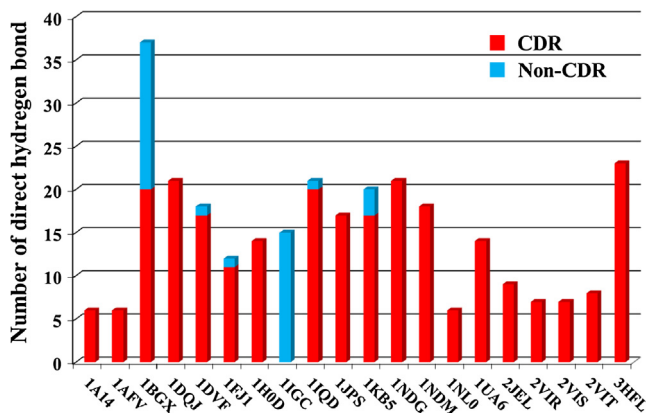


Fig. 4. Number of direct hydrogen bonds between antigen and antibody for each complex.

of antibodies. In particular, the appearance of Tyr at CDR for 1BGX is 20.3% while that in the popular proteins is 2.9%, which is about 7 times higher than that in the popular proteins. In addition, the appearance of Ser at CDR for 1NDM is 25.5% while that in the popular protein is 6.5%. This ratio is about 4 times of that for Ser in the popular proteins.

3.3. Hydrogen bonding at the antigen–antibody interface

All the direct and one-water molecule-mediated hydrogen bonds between antigen and antibody were examined for every complex, using the trajectories of the last 1 ns MD simulation. The number of direct hydrogen bonds between the antigen and the antibody is shown for each complex in Fig. 4. Except for 1IGC, it was clarified that the amino acid residues at CDR of antibody were deeply concerned with the direct hydrogen bonds to the antigen (Fig. S3).

Fig. 5 represents the number of and the classification for physicochemical property of each amino acid residue at CDRs related to the direct hydrogen bonds between antigens and antibodies. The numbers of the direct hydrogen bonds that each kind of residue were involved in was summed up for all the complexes. The total number of hydrogen bonds that the residues at CDRs were involved in was 257, and Tyr shows the highest contribution and also the number of the direct hydrogen bonds was 51 (Fig. 5A). The second was Asn, the third was Asp, and the fourth was Ser (Fig. 5A).

Fig. 6 shows the hydrogen bonds in the 6 complexes; 1AFV, 1UA6, 1DQJ, 1IQD, 2JEL and 2VIR. The dotted line in Fig. 6 represents the hydrogen bond with the shortest distance among all the direct hydrogen bonds between antigen and antibody. Especially, the formations of the strong hydrogen bonds were observed in 1DQJ, 1IQD, and 1KB5. For 1DQJ, the distance between Ser269(H2):HG in the antibody and Asp527:OD2 in the antigen was 2.56 Å. For 1IQD, the distance between Ser31(L1):HG and Gln478:O was 2.58 Å and that between Asp312(H3):OD2 and Ser506:HG was 2.57 Å. For 1KB5, the distance between Ser477(non-CDR):HG in the antibody and Glu25:OE1 in the antigen was 2.53 Å. The 6 complexes in Fig. 6 have a common feature in hydrogen bonding. That is, the amino acid residue responsible for the shortest hydrogen bond is on the heavy chain.

Among the 20 complexes, the maximum number of the direct hydrogen bonds was 37, that was observed in 1BGX, and 20 of the 37 hydrogen bonds are concerned to the residues at CDR. In contrast, the minimum number of the direct hydrogen bonds was 6, which was observed in 1A14, 1AFV, and 1NL0, and all these 6 hydrogen bonds are related to the CDR residues. The details for the direct hydrogen bonds are shown in Table S1 and Tables S2-1 to S2-20.

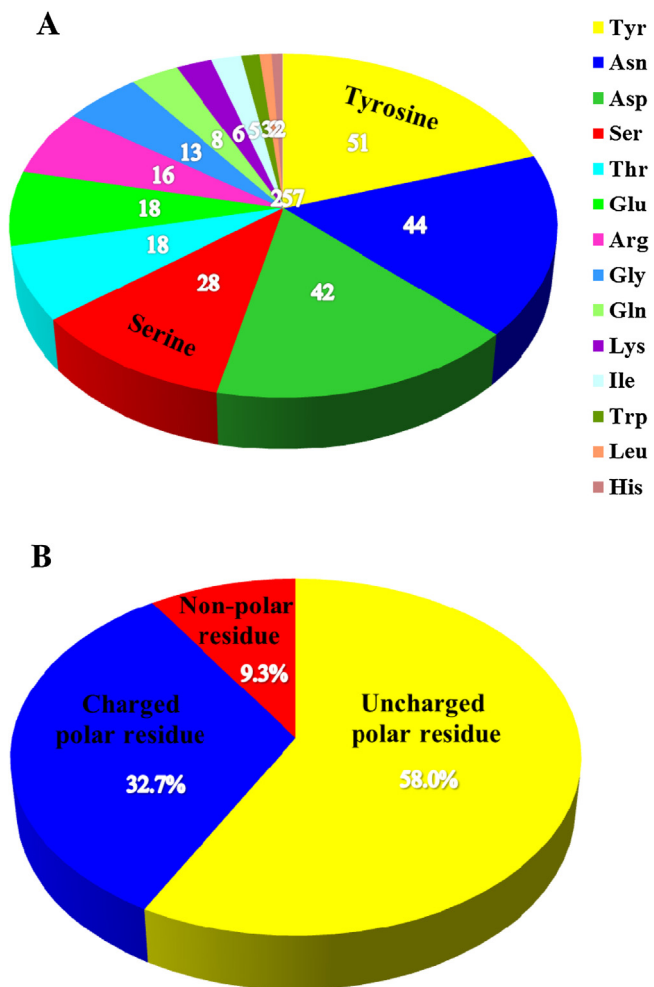


Fig. 5. (A) Number of the direct hydrogen bonds between antigen and antibody, separately counted for each amino acid residue that the direct hydrogen bonds are involved in. (B) Classification of number of hydrogen bonds from the physicochemical property of amino residues.

In 17 out of 20 complexes, the amino acid residue involved in the shortest hydrogen bond was located at CDR of the heavy chain, not the light chain.

Fig. 7 represents the number of one-water-mediated hydrogen bonds. The distances and angles for the hydrogen bonds between water molecules and amino acid residues involved in the antigen–antibody interaction are shown in Tables S3-1 to S3-20. It was suggested in all the twenty complexes that the contribution of water molecules to the antigen–antibody interaction was significant. The number of one water molecule-mediated hydrogen bonds was 2–34 (max value in 1NDM) and the average was 15.5.

3.4. Binding free energy between antigen and antibody

The binding free energies were calculated, using the last 1 ns of MD trajectory acquired at an interval of 10 ps. ΔG_{bind} of the respective complexes and their corresponding energy components are summarized in Table 2. Additionally, the energies for the selected 6 complexes are shown in Fig. 8 as typical instances. The binding free energies for all the twenty complexes are shown in Fig. S4. ΔG_{bind} of all the twenty complexes was negative and ΔG_{bind} ranges from -174.4 kcal/mol (1BGX) to -21.9 kcal/mol (1AFV). In 18 complexes, ΔE_{ele} was lower than ΔE_{vdw} . This fact suggests that ΔE_{ele} significantly contributes to the formation of the antigen–antibody complex. ΔE_{ele} was negative value in 19

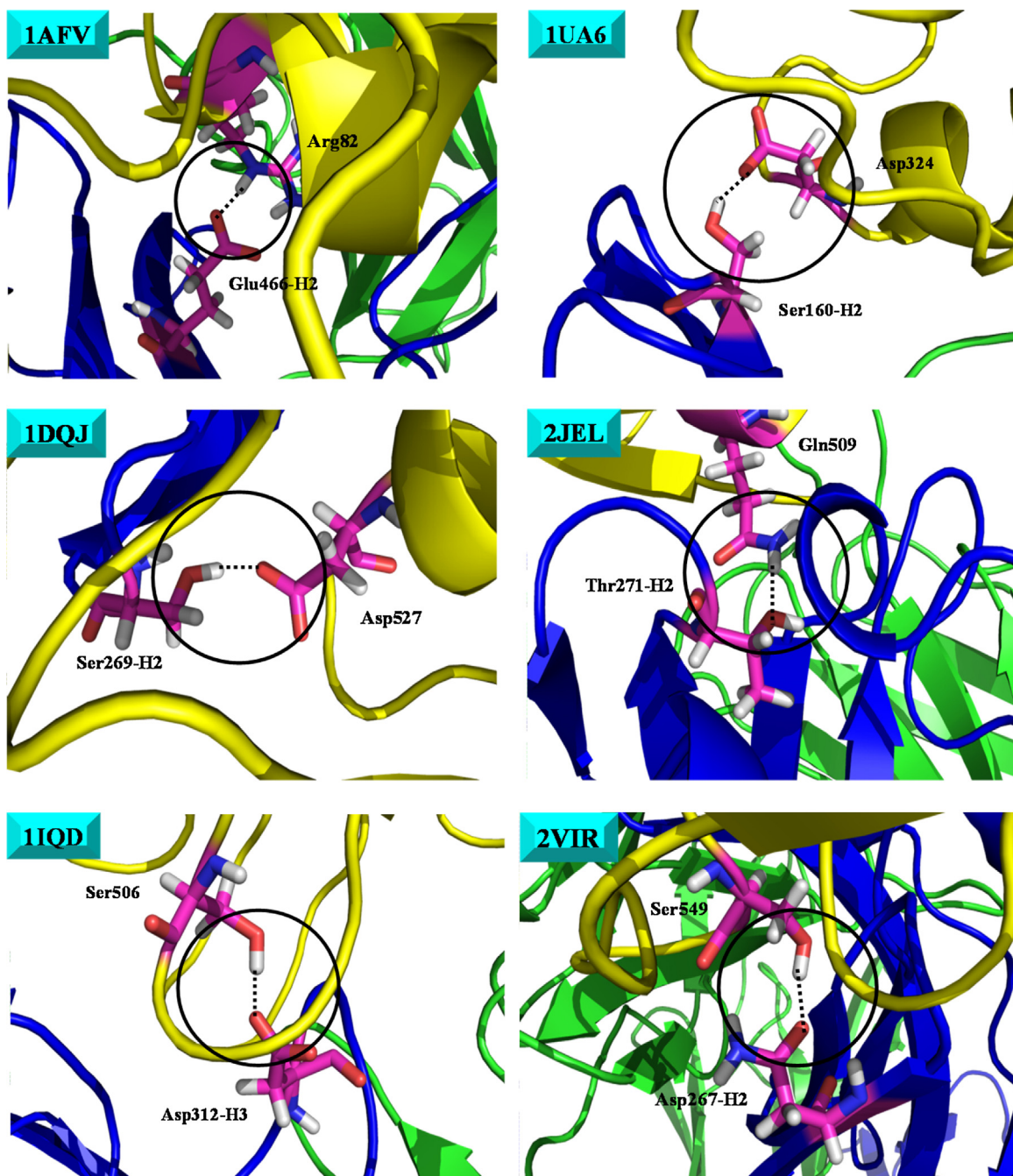


Fig. 6. Structures of the direct and the shortest hydrogen bond between antigen and antibody for the 6 complexes. The dotted line in the circle presents the direct hydrogen bond with the shortest distance among all the direct hydrogen bond.

complexes except for 1KB5, and ΔE_{ele} ranges from -1863.1 kcal/mol (1NLO) to 81.8 kcal/mol (1KB5). On the other hand, ΔE_{vdw} in all the twenty complexes was negative and ranges from -290.0 kcal/mol (1BGX) to -50.3 kcal/mol (1AFV). ΔG_{sol} is positive value except for 1KB5 (-35.4 kcal/mol), suggesting that the energy loss due to the solvation is compensated by the exothermic energies of ΔE_{ele} and ΔE_{vdw} .

3.5. Flexibility of protein structures

Fluctuation of protein structure is closely related to the stability of protein, and protein action is highly correlated with the flexibility of function domains. Hence, B-factor was calculated from the trajectory of MD simulations and compared with that from the

X-ray crystallographic analysis as illustrated in Fig. S5. In Fig. S5, the B-factor values are shown for the respective residues of the antibody in each complex. The averaged B-factor values at CDR loops and non-CDR of antibodies were also calculated as shown in Table 3. Fig. 9 shows the B-factor values for the 6 complexes. The averaged B-factor values at CDR were observed to be lower than those at non-CDR in the 6 complexes. The B-factor values at L1, L2, L3, H1, H2, and H3 of CDR for 1UA6 and 2JEL were small compared to those at non-CDR. In 1UA6, the B-factor values at both CDR and non-CDR were lower than those for the five other antibodies. The B-factors for 1IGC showed the highest values among all the complexes both at CDR and non-CDR, suggesting that the complex for 1IGC is highly flexible. On the other hand, the most rigid one among all the complexes is 1A14 because the average B-factor

Table 2

Binding free energy and its energetic components obtained by the MM-GB/SA method for the 20 complexes.

PDB code	ΔH_{ele} (kcal/mol)	ΔH_{vdw} (kcal/mol)	ΔG_{sol} (kcal/mol)	ΔG_{bind} (kcal/mol)
1A14	-70.3 ± 16.3	-72.3 ± 4.1	105.0 ± 15.1	-37.6 ± 4.3
1AFV	-102.4 ± 20.7	-50.3 ± 3.7	130.9 ± 20.7	-21.9 ± 3.1
1BGX	-644.8 ± 40.2	-290.0 ± 8.4	760.5 ± 34.3	-174.4 ± 9.6
1DQJ	-248.5 ± 23.3	-102.3 ± 5.4	282.9 ± 19.6	-68.0 ± 5.5
1DVF	-145.8 ± 16.2	-102.3 ± 4.1	171.7 ± 13.6	-76.3 ± 4.4
1FJ1	-107.6 ± 22.7	-84.7 ± 4.2	137.5 ± 19.8	-54.9 ± 5.6
1H0D	-147.4 ± 12.4	-81.4 ± 5.2	166.5 ± 11.2	-62.3 ± 4.9
1IGC	-192.9 ± 24.5	-71.5 ± 4.7	207.3 ± 20.9	-57.1 ± 5.5
1IQD	-684.6 ± 25.6	-110.9 ± 5.4	686.8 ± 25.2	-108.6 ± 5.2
1JPS	-433.9 ± 28.3	-110.6 ± 5.9	472.4 ± 25.3	-72.0 ± 5.1
1KB5	81.8 ± 27.7	-114.3 ± 5.1	-35.4 ± 24.3	-67.8 ± 6.1
1NDG	-296.4 ± 17.5	-96.7 ± 4.7	317.5 ± 15.3	-75.6 ± 4.7
1NDM	-296.3 ± 22.8	-104.4 ± 5.6	332.5 ± 21.6	-68.2 ± 5.4
1NL0	-1863.1 ± 87.7	-63.2 ± 3.9	1879.1 ± 85.2	-47.2 ± 4.4
1UA6	-281.5 ± 24.5	-88.8 ± 4.7	315.3 ± 21.0	-55.0 ± 5.5
2JEL	-347.8 ± 17.7	-84.9 ± 3.6	385.7 ± 15.9	-47.0 ± 4.0
2VIR	-134.1 ± 15.3	-69.4 ± 4.3	166.4 ± 14.9	-37.2 ± 3.9
2VIS	-120.7 ± 15.8	-73.3 ± 3.9	151.1 ± 15.6	-42.8 ± 4.6
2VIT	-136.7 ± 18.3	-73.7 ± 7.9	170.2 ± 21.6	-40.2 ± 4.3
3HFL	-318.1 ± 21.2	-99.3 ± 4.9	328.1 ± 17.3	-89.3 ± 5.5

Each energy value presents mean ± standard deviation.

ΔH_{ele} , electrostatic energy; ΔH_{vdw} , van der Walls energy; ΔG_{sol} , solvation energy; ΔG_{bind} , binding free energy.

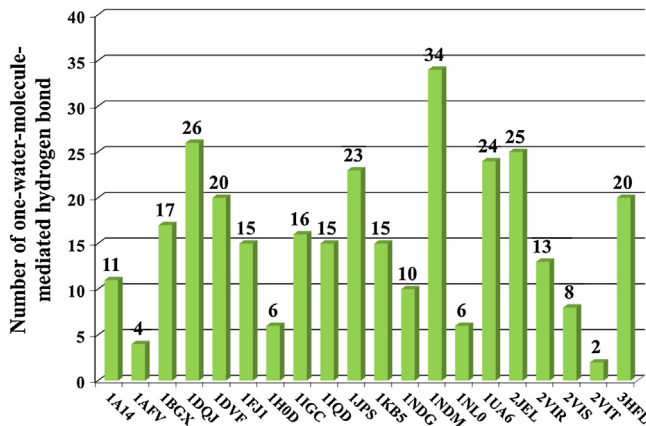


Fig. 7. Number of one-water-molecule-mediated hydrogen bonds concerning to the antigen–antibody interaction.

Table 3

Averaged B-factors of main chain atoms of the respective CDR loops of the antibodies.

PDB code	Averaged B-factor (\AA^2)						
	Non-CDR	L1	L2	L3	H1	H2	H3
1A14	8.5	5.6	6.5	4.5	4.6	7.0	6.3
1AFV	10.5	10.2	8.2	4.6	8.7	6.3	13.3
1BGX	16.3	13.7	13.3	9.1	9.5	11.3	10.7
1DQJ	20.5	14.5	17.4	10.9	20.1	19.1	14.6
1DVF	28.3	12.5	11.0	7.6	13.7	19.3	7.3
1FJ1	20.0	17.7	18.2	11.5	19.1	16.8	17.1
1H0D	16.4	11.7	13.8	7.5	15.6	13.8	12.4
1IGC	32.9	37.0	30.2	24.7	37.1	36.7	37.7
1IQD	22.0	24.3	13.0	9.6	15.1	17.5	10.3
1JPS	15.1	13.2	10.6	7.6	10.1	9.9	7.4
1KB5	14.4	12.0	12.2	7.0	10.7	10.0	7.2
1NDG	26.0	26.2	27.5	16.0	29.7	21.4	18.7
1NDM	23.2	21.5	26.8	11.8	25.2	19.5	13.6
1NL0	20.9	18.3	14.4	13.5	11.2	11.5	9.9
1UA6	9.1	6.4	7.1	4.2	5.0	6.7	4.9
2JEL	17.0	12.0	9.0	7.3	9.8	11.1	7.1
2VIR	18.5	18.4	14.7	12.2	8.2	10.5	18.5
2VIS	17.2	27.9	14.1	11.9	14.4	15.4	15.3
2VIT	18.4	28.0	15.2	16.4	11.3	12.9	21.9
3HFL	17.6	12.4	7.5	6.9	15.0	13.8	8.1

values at L1, L2, H1, and non-CDR are the lowest and those at L2, H2, and H3 are nearly the minimum among all the complexes.

4. Discussion

4.1. Presence of specific amino acid residues in CDR

The uncharged polar residues, Ser and Tyr, are shown to appear at CDR in high rates for all the twenty antibodies. The average appearance ratio of Ser at CDR of the antibodies was 14.6% while 6.5% in the popular proteins and that of Tyr at CDR was 12.0% while 2.9% in the popular proteins. It has been reported that many Ser and Tyr residues exist at CDR to make a large contact with an antigen, and these amino acid residues are intrinsically responsible for molecular recognition [62–64]. Our present result is well consistent with the above reports, suggesting that Ser and Tyr at CDR of antibody play an important role in specific binding and recognition of antigen. In our calculation, Ser and Tyr certainly contribute to the direct and one-water-mediated hydrogen bonds. It was suggested that Tyr at CDRs was deeply related to the formation of the direct hydrogen bond and Ser is also responsible for the direct hydrogen bond as shown in Fig. 5. The direct hydrogen bonds that Tyr and Ser at CDRs were involved in were 51 and 28, respectively. The sum of these two numbers is 31% of the totally 257 direct hydrogen bonds between the antigen–antibody interface (Fig. 5). The reason for the abundance of Tyr and Ser in antibody will be their ability to make stable contact with antigen and to keep water molecules to adjust the space at the antigen–antibody interface. Tyr is involved in not only the hydrogen bonding but also the π – π or CH– π interaction.

4.2. Comparison between antibody and low molecular-weight compound in terms of the number of hydrogen bonds

Hydrogen bonding is one of the most important interactions to induce the biological function of enzymes. A rich hydrogen bond network will stabilize the binding structure of a complex. In the twenty complexes, the number of the direct hydrogen bonds account for from 6 (1A14, 1AFV, and 1NL0) to 37 (1BGX). The average with the standard deviation was 15.0 ± 7.8 . The direct hydrogen bonds between antigen and antibody were observed at CDR in all the complexes except for 1IGC. CDR usually has the loop structure [65–67], and the antigen is obviously positioned outside CDR in

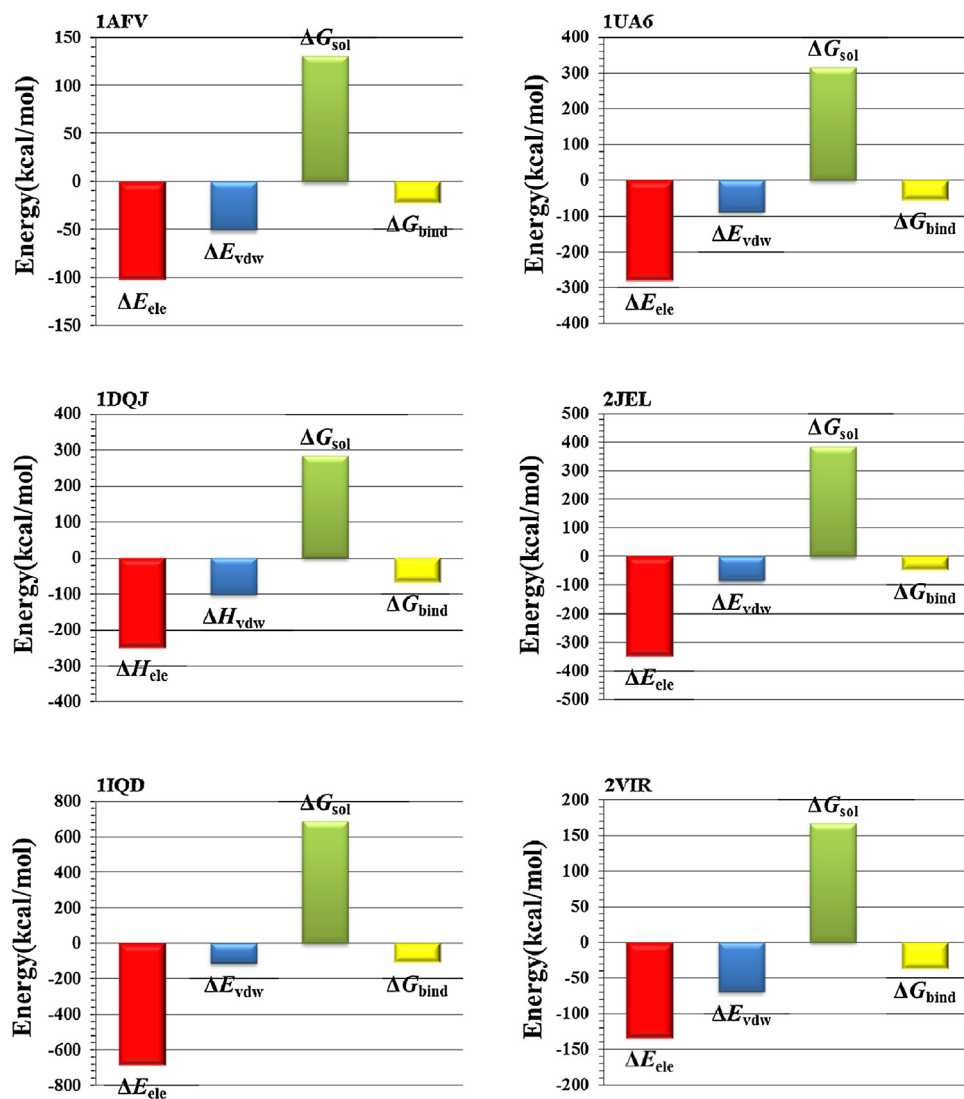


Fig. 8. Binding free energy and its energetic components for the 6 complexes, obtained by the MM-GB/SA method.

1IGC. This unique hydrogen bond network of 1IGC is easily understood from the average structure of Fig. 1, in which the antigen makes a contact with the side part of the antibody. In 1BGX, the loop region of the antibody is positioned around the antigen as seen in Fig. 1. Hence the direct hydrogen bonds were formed between the amino acid residues at CDR and those of the antigen. In addition, in 1BGX, there are also many direct hydrogen bonds at non-CDR of the antibody.

In the 20 complexes, the direct hydrogen bonds between the antigens and their antibodies are composed of both the interactions among charged polar amino acid residues (Arg, Asp, Glu, His, and Lys) and the uncharged polar ones (Asn, Gln, Ser, Thr, and Tyr). The uncharged polar residues are dominantly related to the direct hydrogen bonds and responsible for 58.0% of the total hydrogen bonds (Fig. 5B). In contrast, 32.7% of the total hydrogen bonds are related to the charged polar ones as seen in Fig. 5B. The number of the hydrogen bonds between antigen and antibody were more than those between low molecular-weight compounds and their target proteins [68–70]. For example, Leonis et al. reported from their MD simulation that the complexes of human immunodeficiency virus type 1 (HIV-1) protease and its inhibitors; darunavir, amprenavir, indinavir, and saquinavir, had 5 to 9 direct hydrogen bonds between the enzyme and those low molecular-weight compounds [71]. This number, 5–9, is relatively large for the protein–compound

interaction, because the molecular-weight of the inhibitors for HIV-1 protease is larger than many other oral administrative drugs due to the large binding pocket of the protease. Indeed, the molecular-weights of darunavir, amprenavir, indinavir, and Saquinavir are 548, 506, 614, and 767, respectively. The reason of the difference in number of hydrogen bonds between antibody and chemical compound is that the protein–protein interaction usually has a larger contact area than that in the protein–compound interaction.

According to the classification of hydrogen bonds by Jeffrey [72] and Frey [73], the “single-well hydrogen bond” is very short, typically with an O–O distance of 2.4 to 2.5 Å. The “low-barrier hydrogen bond”, LBHB, is longer than that of the single-well hydrogen bond and the distance ranges from 2.5 to 2.6 Å. The “weak hydrogen bond” is even longer distance than those of the above two sorts of hydrogen bonds and are over 2.6 Å. In 1DQJ, 1IQD, and 1KB5, the formation of the short-distance hydrogen bond that was assumed to be LBHB was observed. Namely, the shortest hydrogen bond distance was 2.56 Å for 1DQJ, 2.57 Å for 1IQD, and 2.53 Å for 1KB5, respectively. The LBHB has a covalent bond-like characteristic and will significantly contribute to the stability of the antigen–antibody complex. It was known that water molecules played an important role in recognition of proteins to their ligands with making water bridges between them and in stabilization of the protein–ligand complex [74,75]. It was clarified from the present study that water

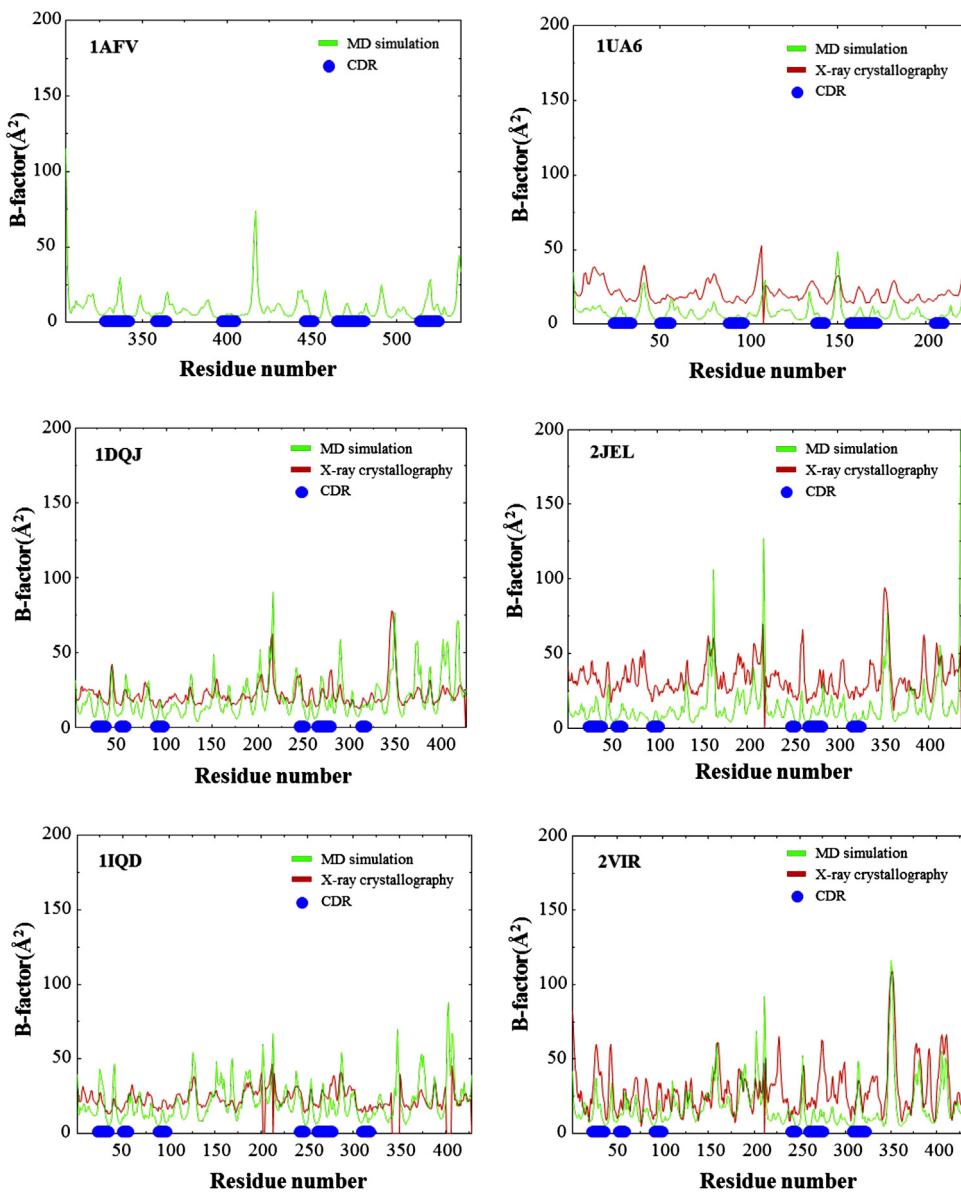


Fig. 9. Averaged B-factors of main chain atoms of antibody in each complex. CDR region is denoted by thick bar at the bottom.

molecules also contributed to the interaction between the antigens and the antibodies. The maximum number of one-water-molecule-mediated hydrogen bonds was 34 and the average was 15.5.

4.3. Comparison between antibody and low molecular-weight compound in terms of binding energy

One hundred of snapshot structures were taken from the MD trajectory for the last 1 ns to calculate binding free energy by MM-GB/SA method. Since ΔG_{bind} for all the 20 complexes were negative, all these complexes are energetically stabilized by binding. It will be interesting to know how degree each complex is stabilized. ΔE_{vdw} , which is one component of ΔG_{bind} , was negative in all the twenty complexes whereas ΔE_{ele} became positive only in 1KB5. The negative ΔG_{sol} in 1KB5 resulted in the lower ΔG_{bind} . In 1KB5, ΔG_{GB} was -17.2 kcal/mol and ΔG_{SA} was -18.2 kcal/mol , both of which were negative values. Hence, the exothermic energies due to the solvation contribute to lower ΔG_{bind} . Interestingly, ΔE_{ele} was lower than ΔE_{vdw} in 18 of the twenty complexes. This fact indicates that the electrostatic interaction rather than

the van der Waals interaction contribute to the formation of the antigen–antibody complex. In contrast, in case of the complex of protein and low molecular-weight compound, ΔE_{vdw} is usually lower than ΔE_{ele} [69,70,76,77] and the van der Waals interaction mainly contributes to the formation of complex. In case of the complexes of HIV-1 protease and its 4 kinds of inhibitors (darunavir, amprenavir, indinavir, and saquinavir), ΔE_{vdw} and ΔE_{ele} for each complex are -66.37 ± 0.07 and -41.82 ± 0.11 , -61.99 ± 0.09 and -50.12 ± 0.13 , -76.40 ± 0.08 and -44.09 ± 0.12 , and -72.31 ± 0.11 and $-36.93 \pm 0.21 \text{ kcal/mol}$, respectively [71]. This difference is attributed to the number of hydrogen bonds because many direct and water molecule-mediated hydrogen bonds are observed at the interface of the antigen–antibody complex.

4.4. Shape complementarity of the antigen–antibody interface

The antigen–antibody interaction is one of the most fundamental examples of molecular recognition. In the molecular recognition, the shape complementarity at the interface of two molecules will be important. The shape correlation (S_C) was calculated for each of

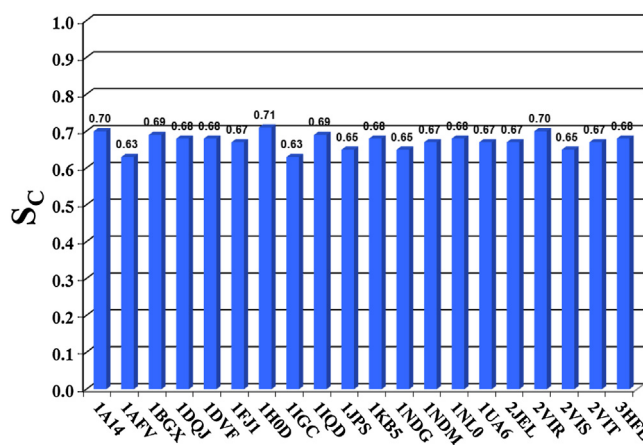


Fig. 10. Shape correlation (S_c) of the antigen–antibody interface for the 20 complexes.

the twenty complexes as shown in Fig. 10. The calculated values were compared with those of the case that a low molecular-weight compound is bound to the target protein, exemplified by HIV-1 protease and its inhibitors [71]. The 4LL3 for darunavir, 3NU3 for amprenavir, 1SDU for indinavir, and 3OXC for saquinavir in PDB were used to calculate S_c for the HIV-1 protease and its inhibitors. The calculation of S_c was performed by an in-house software, SC_calc, which had been coded on the basis of the algorithm proposed by Lawrence and Colman [78]. If two molecules are perfectly fitted to each other, the calculated S_c becomes unity. If two molecules have no structural complementarity, S_c value indicates zero.

Fig. 10 suggests that S_c value ranges from 0.63 to 0.71 for the antigen–antibody complexes. The average with the standard deviation was 0.67 ± 0.02 . S_c for the HIV-1 protease and its inhibitors ranges from 0.68 to 0.71 and the average is 0.70 (darunavir: 0.71, amprenavir: 0.68, indinavir: 0.69, saquinavir: 0.71). The S_c values are almost consistent with the values in the previous report [78]. It is suggested from Fig. 10 that the shape complementarity of the antigen–antibody interface is good, but not so high as low molecular-weight compounds bound to their target proteins. The difference in shape complementarity between the antigen–antibody complex and the inhibitor–enzyme complex implies that the molecular interface is not completely compatible in case of the antigen–antibody complex. The little space due to the incompleteness at the interface is occupied by water molecules, which will result in the better fitting of an antibody to the antigen.

4.5. Difference in the averaged B-factor among complexes

The averaged B-factor in each complex was calculated for the main chain atoms to evaluate the flexibility of the antigen binding site. Additionally, the average B-factor at CDR was compared with that at non-CDR. The averaged B-factor values at CDR are generally lower than those at non-CDR in the 20 complexes except for 1IGC. The L1, L2, L3, H1, H2, and H3 loops of CDR for 1BGX, 1DQJ, 1DVF, 1FJ1, 1HOD, 1JPS, 1KB5, 1NLO, 1UA6, 2JEL, and 3HFL indicated low averaged B-factor values than those at non-CDR. The antibody for 1A14 will form a stable interface with the antigen compared to the other complexes because the average B-factor values at L1, L2, H1, and non-CDR are the lowest among all the complexes (5.6, 6.5, 4.6, and 8.5 \AA^2 , respectively) and those at L3, H2, and H3 are close to the minimum (4.2, 6.3, and 4.9 \AA^2 , respectively). On the other hands, the antibody for 1IGC form a flexible interface because the averaged B-factor at both CDR and non-CDR showed the highest among all twenty complexes and additionally the averaged B-factors at CDR tend to be higher than those at non-CDR. This large B-factors at CDR

of 1IGC is easily understood from the binding structure in which the antigen is attached to the outside of the CDR.

A comparison in B-factor profile with respect to the residues between MD simulation and X-ray crystal analysis shows a remarkable similarity in all complexes except for 1AFV (Fig. S5). It is interesting to note that there exists a fine compatibility in flexibility between simulation and crystallography, while the B-factor is calculated by the average over time for MD simulation whereas by the average over space for X-ray crystallography.

Computational result of MD simulation depends on the initial structure that is set at the starting point of the simulation, to some extent. The initial structure is usually built by referring the crystal structure. Even for crystal structures, there exists a dependency on the experimental condition as pointed out by a recent study [79]. Therefore, using several models will be safe to extract the fundamental properties of the protein molecules. In this study, twenty kinds of the complexes were used to deduce the feature in the antigen–antibody interaction.

5. Conclusions

MD simulations were carried out for twenty kinds of the antigen–antibody complexes to investigate the characteristic of the interactions between antigens and antibodies. It was clarified from the present simulations that (i) the uncharged polar residues, especially Ser and Tyr, are likely to appear at CDR of the antibodies in high presence ratios. Tyr at CDRs significantly contributed to the direct hydrogen bonds between antigen and antibody. By counting the number of the direct hydrogen bonds that each residue is involved in, Tyr was shown to have the highest contribution for hydrogen bonding, and Ser was the fourth. Additionally, the sum of the direct hydrogen bonds that Tyr and Ser were involved in occupied 31% of the total hydrogen bonds. Moreover, the short-distance hydrogen bond, which was assumed to be “low-barrier hydrogen bond”, was observed in three complexes. Ser is responsible for the two short-distance hydrogen bonds out of the three. Hence, Ser and Tyr at CDR of antibody play a critical role in binding to antigen. (ii) In the binding free energy calculation, the electrostatic energy, ΔE_{ele} , was lower than the van der Waals energy, ΔE_{vdw} , in almost all the complexes, which suggests that ΔE_{ele} rather than ΔE_{vdw} largely contributes to the antigen–antibody binding, contrary to the interaction between the low molecular-weight compounds and their target proteins. These findings will be helpful to design an antibody with a high specificity and a high affinity to the target antigen.

Acknowledgments

Calculations were performed at Research Center for Computational Science, Okazaki, Japan, and Information Technology Center of the University of Tokyo, and also by the high-performance computer system at Institute for Media Information Technology of Chiba University. A part of this work was supported by Grant-in-Aid for Scientific Research (C) (#24590548) from Japan Society for the Promotion of Science (JSPS).

Appendix A. Supplementary data

Supplementary data associated with this article can be found, in the online version, at <http://dx.doi.org/10.1016/j.jmgm.2014.07.005>.

References

- [1] M.E. Rodrigues, A.R. Costa, M. Henriques, J. Azeredo, R. Oliveira, Technological progresses in monoclonal antibody production systems, *Biotechnol. Prog.* 26 (2010) 332–351.

- [2] J. Huamg, J. Liang, Q. Tang, Z. Wang, L. Chen, J. Zhu, Z. Feng, An active murine-human chimeric Fab antibody derived from *Escherichia coli*, potential therapy against over-expressing VEGFR2 solid tumors, *Appl. Microbiol. Biotechnol.* 91 (2011) 1341–1351.
- [3] J. Banerjee, Antibodies are challenged, *Indian J. Med. Sci.* 64 (2010) 144–147.
- [4] J.M. Reichert, Antibodies to watch in 2013, *MAbs* 5 (2013) 1–5.
- [5] J.C. Pai, J.N. Sutherland, J.A. Maynard, Progress towards recombinant anti-infective antibodies, *Recent Pat. Antiinfect. Drug Discov.* 4 (2009) 1–17.
- [6] I. Kumagai, K. Tsumoto, Antigen-Antibody Binding, Encyclopedia of Life Sciences, Nature Publishing Group, New Jersey(NJ), US, 2001, pp. 1–7, www.els.net
- [7] E.P. Altshuler, V. Serebryanaya, A.G. Katrukha, Generation of recombinant antibodies and means for increasing their affinity, *Biochemistry (Moscow)* 75 (2010) 1584–1605.
- [8] Y. Li, G. Parry, L. Chen, J.A. Callahan, D.E. Shaw, E.J. Meehan, A.P. Mazar, M. Hung, An anti-urokinase plasminogen activator receptor (uPAR) antibody: crystal structure and binding epitope, *J. Mol. Biol.* 365 (2007) 1117–1129.
- [9] A. Desmyter, K. Decanniere, S. Muyldermans, L. Wyns, Antigen specificity and high affinity binding provided by one single loop of a camel single-domain antibody, *J. Biol. Chem.* 276 (2001) 26285–26290.
- [10] M. Torres, A. Casadevall, The immunoglobulin constant region contributes to affinity and specificity, *Trends Immunol.* 29 (2008) 91–97.
- [11] R.L. Malby, A.J. McCoy, A.A. Kortt, P.J. Hudson, P.M. Colman, Three-dimensional structures of single-chain Fv-neuraminidase complexes, *J. Mol. Biol.* 279 (1998) 901–910.
- [12] A.A. Kortt, E. Nice, L.C. Gruen, Analysis of the binding of the Fab fragment of monoclonal antibody NC10 to influenza virus N9 neuraminidase from tern and whale using the BIACore biosensor: effect of immobilization level and flow rate on kinetic analysis, *Anal. Biochem.* 273 (1999) 133–141.
- [13] J.T. Lee, G.M. Air, Contacts between influenza virus N9 neuraminidase and monoclonal antibody NC10, *Virology* 300 (2002) 255–268.
- [14] C. Momany, L.C. Kovari, A.J. Prongay, W. Keller, R.K. Gitti, B.M. Lee, A.E. Gorbalenya, L. Tong, J. McClure, L.S. Ehrlich, M.F. Summers, C. Carter, M.G. Rossman, Crystal structure of dimeric HIV-1 capsid protein, *Nat. Struct. Biol.* 3 (1996) 763–770.
- [15] S.M. Malbet, C.B. Colominas, A. Novelli, N. Battaï, N. Piga, V. Cheynet, F. Mallet, S. Cusack, Mutual conformational adaptations in antigen and antibody upon complex formation between an Fab and HIV-1 capsid protein p24, *Structure* 8 (2000) 1069–1077.
- [16] R. Murali, D.J. Sharkey, L. Daiss, H.M. Murthy, Crystal structure of Taq DNA polymerase in complex with an inhibitory Fab: the Fab is directed against an intermediate in the helix coil dynamics of the enzyme, *Proc. Natl. Acad. Sci. U. S. A.* 95 (1998) 12562–12567.
- [17] Y. Li, H. Li, S.J. Smith-Gill, R.A. Mariuzza, Three-dimensional structures of the free and antigen-bound Fab from monoclonal antilysozyme antibody HyHEL-63, *Biochemistry* 39 (2000) 6296–6309.
- [18] Y. Li, M. Urrutia, S.J. Smith-Gill, R.A. Mariuzza, Dissection of binding interactions in the complex between the anti-lysozyme antibody HyHEL-63 and its antigen, *Biochemistry* 42 (2003) 11–22.
- [19] Y. Li, H. Li, F. Yang, S.J. Smith-Gill, R.A. Mariuzza, Crystal structure of Fab fragment of antibody HyHEL-8 complexed with its antigen lysozyme, *Nat. Struct. Biol.* 10 (2003) 482–488.
- [20] T. Nakanishi, K. Tsumoto, A. Yokota, H. Kondo, I. Kumagai, Critical contribution of VH–VL interaction to reshaping of an antibody: the case of humanization of anti-lysozyme antibody, *HyHEL-10*, *Protein Sci.* 17 (2008) 261–270.
- [21] S. Mohan, K. Kouranti, K.A. Schick, C. Uehara, C.A. Lipschultz, M. Accihone, M.E. DeSantis, S.J. Smith-Gill, R.C. Willson, Association energetics of cross-reactive and specific antibodies, *Biochemistry* 48 (2009) 1390–1398.
- [22] Y. Li, H. Li, F. Yang, S.J. Smith-Gill, R.A. Mariuzza, X-ray snapshots of the maturation of an antibody response to a protein antigen, *Nat. Struct. Biol.* 10 (2003) 482–488.
- [23] S. Mohan, N. Sinha, S.J. Smith-Gill, Modeling the binding sites of anti-hen egg white lysozyme antibodies HyHEL-8 and HyHEL-26: an insight into the molecular basis of antibody cross-reactivity and specificity, *Biophys. J.* 85 (2003) 3221–3236.
- [24] I. Kumagai, Y. Nishimiya, H. Kondo, K. Tsumoto, Structural consequences of target epitope-directed functional alteration of an antibody, *J. Biol. Chem.* 278 (2003) 24929–24936.
- [25] M. Accihonea, C. Lipschultz, M. DeSantis, A. Shamuganathana, M. Li, A. Wlodawer, S. Tarasov, S.J. Smith-Gill, Light chain somatic mutations change thermodynamics of binding and water coordination in the HyHEL-10 family of antibodies, *Mol. Immunol.* 47 (2009) 457–464.
- [26] A. Yokota, K. Tsumoto, M. Shiroishi, T. Nakanishi, H. Kondo, I. Kumagai, Contribution of asparagine residues to the stabilization of a proteinaceous antigen–antibody complex, HyHEL-10-hen egg white lysozyme, *J. Biol. Chem.* 285 (2010) 7686–7696.
- [27] G.H. Cohen, E.W. Silvertown, E.A. Padlan, F. Dyda, J.A. Wibbenmeyer, R.C. Willson, D.R. Davies, Water molecules in the antibody–antigen interface of the structure of the Fab HyHEL-5–lysozyme complex at 1.7 Å resolution: comparison with results from isothermal titration calorimetry, *Acta Crystallogr. D: Biol. Crystallogr.* 61 (2005) 628–633.
- [28] M. Dlugosz, J.M. Antosiewicz, J. Trylska, pH-dependent association of proteins: the test case of monoclonal antibody HyHEL-5 and its antigen hen egg white lysozyme, *J. Phys. Chem. B* 113 (2009) 15662–15669.
- [29] B.C. Braden, B.A. Fields, X. Ysern, W. Dall'Acqua, F.A. Goldbaum, R.J. Poljak, R.A. Mariuzza, Crystal structure of an Fv–Fvidiotope–anti-idiotope complex at 1.9 Å resolution, *J. Mol. Biol.* 264 (1996) 137–151.
- [30] F.A. Goldbaum, A. Velikovsky, W. Dall'Acqua, C.A. Fossati, B.A. Fields, B.C. Braden, R.J. Poljak, R.A. Mariuzza, Characterization of anti-anti-idiotypic antibodies that bind antigen and an anti-idiotype, *Proc. Natl. Acad. Sci. U. S. A.* 94 (1997) 8697–8701.
- [31] W. Ding, X. Huang, X. Yang, J.J. Dunn, B.J. Luft, S. Koide, C.L. Awson, Structural identification of a key protective B-cell epitope in Lyme disease antigen OspAk, *J. Mol. Biol.* 302 (2000) 1153–1164.
- [32] M. Nassal, C. Skamel, P.A. Kratz, R. Wallich, T. Stehle, M.M. Simon, A fusion product of the complete *Borrelia burgdorferi* outer surface protein A (OspA) and the hepatitis B virus capsid protein is highly immunogenic and induces protective immunity similar to that seen with an effective lipitated OspA vaccine formula, *Eur. J. Immunol.* 35 (2005) 655–665.
- [33] G.B. Chavali, A.C. Papageorgiou, K.A. Olson, J.W. Fett, G. Hu, R. Shapiro, K.R. Acharya, The crystal structure of human angiogenin in complex with an anti-tumor neutralizing antibody, *Structure* 11 (2003) 875–885.
- [34] J.P. Derrick, D.B. Wigley, The third IgG-binding domain from streptococcal protein G: an analysis by X-ray crystallography of the structure alone and in a complex with Fab, *J. Mol. Biol.* 243 (1994) 906–918.
- [35] G.E. Khouri, C.R. Lowe, A biomimetic protein G affinity adsorbent: an Ugi ligand for immunoglobulins and Fab fragments based on the third IgG-binding domain of protein G, *J. Mol. Recognit.* 26 (2013) 190–200.
- [36] P.C. Spiegel, M. Jacquemin, J.R. Saint-Remy, B.L. Stoddard, K.P. Pratt, Structure of a factor VIII C2 domain–immunoglobulin G4k Fab complex: identification of an inhibitory antibody epitope on the surface of factor VIII, *Blood* 98 (2001) 13–19.
- [37] J.D. Dimitrov, L.T. Roumenina, J.-L. Plantier, S. Andre, D. Sabouard, Y. Meslier, C. Planchais, M. Jacquemin, J.-M. Saint-Remy, B.P. Antanasov, S.V. Kaveri, S. Lacroix-Desmazes, A human FVIII inhibitor modulates FVIII surface electrostatics at a VWF-binding site distant from its epitope, *J. Thromb. Haemost.* 8 (2010) 1524–1531.
- [38] K. Faehlber, D. Kirchhofer, L. Presta, R.F. Kelley, Y.A. Muller, The 1.85 Å resolution crystal structures of tissue factor in complex with humanized Fab D3h44 and of free humanized Fab D3h44: revisiting the solvation of antigen combining sites, *J. Mol. Biol.* 313 (2001) 83–97.
- [39] C. Eigenbrot, Y.G. Meng, R. Krishnamurthy, M.T. Lipari, L. Presta, B. Devaux, T. Wong, P. Moran, S. Bullens, D. Kirchhofer, Structural insight into how an anti-idiotypic antibody against D3h44 (anti-tissue factor antibody) restores normal coagulation, *J. Mol. Biol.* 331 (2003) 433–446.
- [40] D. Housset, G. Mazza, C. Grégoire, C. Piras, B. Malissen, J.C. Fontecilla-Camps, The three-dimensional structure of a T-cell antigen receptor VαVβ heterodimer reveals a novel arrangement of the Vβ domain, *EMBO J.* 16 (1997) 4205–4216.
- [41] G. Mazza, D. Housset, C. Piras, C. Grégoire, J.C. Fontecilla-Camps, B. Malissen, Structural features of the interaction between an anti-clonotypic antibody and its cognate T-cell antigen receptor, *J. Mol. Biol.* 287 (1999) 773–780.
- [42] M. Huang, B.C. Furie, B. Furie, Crystal structure of the calcium-stabilized human factor IX Gla domain bound to a conformation-specific anti-factor IX antibody, *J. Biol. Chem.* 279 (2004) 14338–14346.
- [43] X. Shi, Y. Li, C. Bian, G. Zhao, M. Huang, Crystallization of an anti-factor IX antibody and its complex, *Acta Crystallogr. D: Biol. Crystallogr.* 61 (2005) 701–703.
- [44] L. Prasad, E.B. Waygood, J.S. Lee, L.T.J. Delbaere, The 2.5 Å resolution structure of the Jel42 Fab fragment/HPr complex, *J. Mol. Biol.* 280 (1998) 829–845.
- [45] J.E. Smallshaw, F. Georges, J.S. Lee, E.B. Waygood, Synthesis, cloning and expression of the single-chain Fv gene of the HPr-specific monoclonal antibody, Jel42: determination of binding constants with wild-type and mutant HPrs, *Protein Eng.* 12 (1999) 623–630.
- [46] D. Fleury, S.A. Wharton, J.J. Skehel, M. Knossow, T. Bizebard, Antigen distortion allows influenza virus to escape neutralization, *Nat. Struct. Biol.* 5 (1998) 119–123.
- [47] M.J. Edwards, N.J. Dimmock, A haemagglutinin (HA1)-specific FAb neutralizes influenza A virus by inhibiting fusion activity, *J. Gen. Virol.* 82 (2001) 1387–1395.
- [48] P. Lee, R. Yoshida, D.C. Ekiert, N. Sakai, Y. Suzuki, A. Takada, I.A. Wilson, Hetero-subtypic antibody recognition of the influenza virus hemagglutinin receptor binding site enhanced by avidity, *Proc. Natl. Acad. Sci. U. S. A.* 109 (2012) 17040–17045.
- [49] M.I. Mahmood, Y. Matsuo, S. Neya, T. Hoshino, Computational analysis on the binding of epitope peptide to human leukocyte antigen class I molecule A*2402 subtype, *Chem. Pharm. Bull.* 59 (2011) 1254–1262.
- [50] G. Scarabelli, G. Morra, G. Colombo, Predicting interaction sites from the energetics of isolated proteins: a new approach to epitope mapping, *Biophys. J.* 98 (2010) 1966–1975.
- [51] D.A. Case, T.E. Cheatham III, T. Darden, H. Gohlke, R. Luo, K.M. Merz Jr., A. Onufriev, C. Simmerling, B. Wang, R. Woods, The Amber biomolecular simulation programs, *J. Comput. Chem.* 26 (2005) 1668–1688.
- [52] B.R. Brooks, R.E. Bruckolieri, B.D. Olafson, D.J. States, S. Swaminathan, M. Karplus, CHARMM: a program for macromolecular energy, minimization, and dynamics calculations, *J. Comput. Chem.* 4 (1983) 187–217.
- [53] W.L. DeLano, The PyMOL Molecular Graphics System, Schrödinger, LLC, 2012.
- [54] D. Voet, J.G. Voet, *Biochemistry*, 4th ed., John Wiley & Sons Inc., New Jersey, 2011, pp. 68–69.
- [55] SIB, UniProtKB/Swiss-Prot Protein Knowledgebase Release 2014_04 Statistics, Swiss Institute of Bioinformatics, Lausanne, Switzerland, 2014, available at: <http://www.expasy.ch/sprot/renotes/relstat.html>
- [56] P.A. Kollman, I. Massova, C. Reyes, B. Kuhn, S. Huo, L. Chong, M. Lee, T. Lee, Y. Duan, E. Wang, O. Donini, P. Cleplak, J. Srinivasan, D.C. Case, T.E. Cheatham III, Calculating structures and free energies of complex molecules:

- combining molecular mechanics and continuum models, *Acc. Chem. Res.* 33 (2000) 889–897.
- [57] H. Gohlke, D.A. Case, Converging free energy estimates: MM-PB(GB)SA studies on the protein–protein complex Ras–Raf, *J. Comput. Chem.* 25 (2004) 238–250.
- [58] A.D. Onufriev, D.A. Case, Exploring protein native states and large-scale conformational changes with a modified generalized born model, *Proteins* 55 (2004) 383–394.
- [59] J. Weiser, P.S. Shenkin, W.C. Still, Approximates atomic surfaces from linear combinations of pairwise overlaps, *J. Comput. Chem.* 20 (1999) 217–230.
- [60] V. Zoete, O. Michielin, M. Karplus, Relation between sequence and structure of HIV-1 protease inhibitor complexes: a model system for the analysis of protein flexibility, *J. Mol. Biol.* 315 (2002) 21–52.
- [61] K. Mori, M. Hata, S. Neya, T. Hoshino, Common semi-open conformations of Mg²⁺-free Ras, Rho, Rab, Arf, and Ran proteins combined with GDP and their similarity with GEF-bound forms, *J. Am. Chem. Soc.* 127 (2005) 15127–15137.
- [62] F.A. Fellouse, C. Wiesmann, S.S. Sidhu, Synthetic antibodies from a four-amino-acid code: a dominant role for tyrosine in antigen recognition, *Proc. Natl. Acad. Sci. U. S. A.* 101 (2004) 12467–12472.
- [63] F.A. Fellouse, B. Li, D.M. Compaan, A.A. Peden, S.G. Hymowitz, S.S. Sidhu, Molecular recognition by a binary code, *J. Mol. Biol.* 348 (2005) 1153–1162.
- [64] F.A. Fellouse, P.A. Barthelemy, R.F. Kelley, S.S. Sidhu, Tyrosine plays a dominant functional role in the paratope of a synthetic antibody derived from a four amino acid code, *J. Mol. Biol.* 357 (2006) 100–114.
- [65] V. Morea, A. Tramontano, M. Rustici, C. Chothia, A.M. Lesk, Conformations of the third hypervariable region in the VH domain of immunoglobulins, *J. Mol. Biol.* 275 (1998) 269–294.
- [66] B.D. Sellers, J.P. Nilmeier, M.P. Jacobson, Antibodies as a model system for comparative model refinement, *Proteins* 78 (2010) 2490–2505.
- [67] B. North, A. Lehmann, R.L. Dunbrack Jr., A new clustering of antibody CDR loop conformations, *J. Mol. Biol.* 406 (2011) 228–256.
- [68] C. Yan, Z. Xiu, X. Li, S. Li, C. Hao, H. Teng, Comparative molecular dynamics simulations of histone deacetylase-like protein: binding modes and free energy analysis to hydroxamic acid inhibitors, *Proteins* 73 (2008) 134–149.
- [69] R. Xiong, X.M. Cai, J. Wei, P.Y. Ren, Some insights into the binding mechanism of Aurora B kinase gained by molecular dynamics simulation, *J. Mol. Model.* 18 (2012) 4591–4601.
- [70] H. Chen, Y. Zhang, L. Li, J.G. Han, Probing ligand-binding modes and binding mechanisms of benzoxazole-based amide inhibitors with soluble epoxide hydrolase by molecular docking and molecular dynamics simulation, *J. Phys. Chem. B* 116 (2012) 10219–10233.
- [71] G. Leonis, T. Steinbrecher, M.G. Papadopoulos, A contribution to the drug resistance mechanism of darunavir, amprenavir, indinavir, and saquinavir complexes with HIV-1 protease due to flap mutation I50V: a systematic MM-PBSA and thermodynamic integration study, *J. Chem. Inf. Model.* 53 (2013) 2141–2153.
- [72] G.A. Jeffrey, *An Introduction to Hydrogen Bonding*, Oxford University Press, Oxford, England, 1997.
- [73] P.A. Frey, A. Kohen, H.H. Limbach, *Isotope Effects in Chemistry and Biology*, CRC Press, Boca Raton, FL, 2006, pp. 975–993.
- [74] M.L. Raymer, P.C. Sanschagrin, W.F. Punch, S. Venkataraman, E.D. Goodman, L.A. Kuhn, Predicting conserved water-mediated and polar ligand interactions in proteins using a K-nearest-neighbors genetic algorithm, *J. Mol. Biol.* 265 (1997) 445–464.
- [75] G.A. Ross, G.M. Morris, P.C. Biggin, Rapid and accurate prediction and scoring of water molecules in protein binding sites, *PLoS ONE* 7 (2012) 1–13.
- [76] S. Matsuyama, A. Aydan, H. Ode, M. Hata, W. Sugiura, T. Hoshino, Structural and energetic analysis on the complexes of clinically isolated subtype C HIV-1 proteases and approved inhibitors by molecular dynamics simulation, *J. Phys. Chem. B* 114 (2010) 521–530.
- [77] P. Zhao, S.K. Chen, Y.H. Cai, X. Lu, Z. Li, Y.K. Cheng, X.H. Zhang, X. Hu, X. He, H.B. Luo, The molecular basis for the inhibition of phosphodiesterase-4D by three natural resveratrol analogs: isolation, molecular docking, molecular dynamics simulations, binding free energy, and bioassay, *Biochim. Biophys. Acta* 1834 (2013) 2089–2096.
- [78] M.C. Lawrence, P.M. Colman, Shape complementarity at protein/protein interfaces, *J. Mol. Biol.* 234 (1993) 946–950.
- [79] F. Qi, S. Fudo, S. Neya, T. Hoshino, A cluster analysis on the structural diversity of protein crystals, exemplified by human immunodeficiency virus type 1 protease, *Chem. Pharm. Bull.* 62 (2014) 568–577.